Evolution of Bubble Length Distributions in Three-Phase Fluidized Beds

S. L. P. Lee
A. Soria
H. I. de Lasa
Chemical Reactor Engineering Centre
Faculty of Engineering Science
The University of Western Ontario
London, Ontario, Canada N6A 5B9

Three-phase fluidization is an operation that has been applied to many chemical processes. The performance of a three-phase fluidized bed reactor is highly influenced by the bubble behavior. For example, gas bubbles affect bed expansion, bed mixing, gas holdup, particle entrainment, and mass transfer among the three phases. Therefore, the knowledge of the gas holdup, bubble velocity, bubble size, and its distribution, is very important in order to understand the behavior of this type of reactor.

The aim of the present study is the description of the steady-state evolution processes of the average value and the distribution of bubble lengths in a column with solid particles whose diameter is smaller than the so-called critical particle size, (Lee et al., 1974), which is around 3 mm for the air–water–glass beads system. Bubble length distributions are obtained from *in situ* fiber optic probe measurements throughout the fluidized bed. The evolution of bubble length distributions is studied under various operating conditions. The bubble flow regimes are identified objectively by studying, under steady-state operation, the bubble length mappings (functions of both axial and radial positions) in the fluidized bed.

Experimental Setup

The experiments were performed in a cylindrical fluidized bed of 0.2 m ID. Air, water, and 250 μm glass beads were used as the gas, liquid, and solid phases. The details of the apparatus and the procedure of experiments were described in a previous publication by Lee and de Lasa (1987). However, a different gas injection system was used in this study. A single injector of 1.25 cm OD was positioned at the center of the distributor. The tip of the injector was covered by a porous metal plate, pore size 40 μm, to generate relatively small bubbles.

The gas bubbles were measured by two optical fiber probes. The measuring probes were made of two parallel fibers fused together at the ends to form a spherical tip, where the gas bubbles were detected. The details of the probes were described by Lee and de Lasa (1989). The bubble velocity measurements were carried out at four different axial heights, 0.075, 0.225, 0.375, and 0.525 m above the distributor. At each axial location the measurements were performed at nine positions across the radius, $r/R = 0, \pm 0.25, \pm 0.5, \pm 0.75$, and ± 0.875.

Data Analysis

The bubble velocity was obtained by dividing the probe separation, 0.94 cm, by the time shift between the signals from the two probes. Once the bubble velocity was defined, the bubble length was calculated by multiplying the bubble velocity and the duration of the bubble signal. Careful screening of the original data was performed to check the similarity between the signals from the two probes. These checkings include rise times, fall times, durations, maximum values, variances, and cross correlations of the two signals. The details of the analysis for signal discrimination were described by Lee et al. (1984).

The Marquardt optimization technique was used in obtaining the parameters for different bubble length distribution functions. The normal, the truncated normal, and the log normal distributions were tested. The truncated normal distribution gave the best fit to the experimental data while the normal and the log normal distribution functions were revealed to be unsuitable.

If the distribution function is truncated at zero, the probability density function, the mean and the variance are given as follows:

$$f(\ell) = \frac{1}{\Phi(\mu/\sigma)\,\sigma\sqrt{2\pi}}\, e^{-(\ell-\mu)^2/2\sigma} \qquad (1)$$

The present address of A. Soria is Departamento de I.P.H., Universidad Autónoma Metropolitana, 09340 México, D.F.

and

$$E(\ell) = \mu + \frac{\sigma}{\Phi(\mu/\sigma)\sqrt{2\pi}} e^{-(\mu/\sigma)^2/2} \quad (2)$$

$$\text{Var}(\ell) = \sigma^2 - \frac{\mu\sigma}{\Phi(\mu/\sigma)\sqrt{2\pi}} e^{-(\mu/\sigma)^2/2} - \left[\frac{\sigma}{\Phi(\mu/\sigma)\sqrt{2\pi}}\right]^2 e^{-(\mu/\sigma)^2} \quad (3)$$

Results and Discussion

Since a single gas bubble injector was placed at the center of the grid, a conical shape of gas bubble trajectories close to the grid was observed. The jet effect was very pronounced near the grid level, $z = 7.5$ cm, where gas bubbles were observed only at the center of the column. The gas bubbles were then dispersed laterally as they rose in the fluidized bed.

The bubble coalescence and the bubble dispersion regimes can be distinguished by the evolution of bubble length distribution in the fluidized bed. The phenomenon of bubble breakage is indicated by a progressive decrease in the mean bubble length and the width of the bubble length distributions for the conditions shown in Figure 1.

Grid level

Bubble length distributions near the grid, $z = 7.5$ cm—called further in this paper grid level bubble length distributions—under different operating conditions were considered. Operating variables and statistical parameters for these distribution functions are listed in Table 1. It can be observed in Figure 2 that at low liquid velocity (0.39 and 0.78 cm/s), the bubble length distribution was narrower (standard deviations: 0.66 and 0.71 cm) and with a tail toward the bigger sizes. Flat and wide grid level bubble length distributions (standard deviations: 0.85 and 1.03 cm) were observed at high liquid velocities (1.17 and 1.56 cm/s). High gas velocities also contributed to a larger mean bubble length and a wider grid level bubble length distribution, as shown in Table 1. For example, at $V_L = 0.39$ cm/s, the mean and standard deviation of the distribution function, respectively, increased from 1.07 and 0.66 cm to 1.93 and 1.28 cm when V_G was increased from 0.6 to 1.33 cm/s. Further increase in gas velocity only resulted in an even larger standard deviation of the distribution function. Considering this information, it appears that two distinct types of grid level bubble length distributions

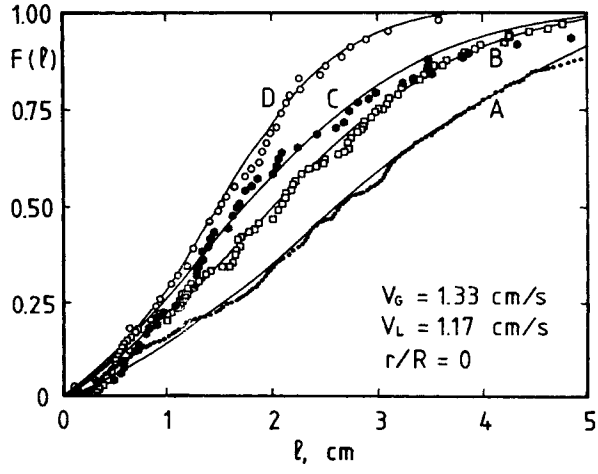

Figure 1. Cumulative bubble length distributions in three-phase fluidized bed.

$V_G = 1.33$ cm/s, $V_L = 1.17$ cm/s, $r/R = 0$, $z = 22.5$ cm. *A*, *B*, *C*, and *D* represent $z = 7.5$, 22.5, 37.5, 52.5 cm, respectively

Table 1. Bubble Length Distribution at Different Heights and $r/R = 0$

V_G cm/s	V_L cm/s	z cm	μ cm	σ cm	$E(\ell)$ cm	$\text{Var}(\ell)^{1/2}$ cm
0.6	0.39	7.5	0.82	0.84	1.07	0.66
		22.5	1.27	1.14	1.55	0.93
		37.5	1.62	0.84	1.67	0.78
		52.5	1.45	0.65	1.47	0.62
0.6	0.78	7.5	1.09	0.83	1.25	0.71
		22.5	1.44	0.91	1.55	0.81
		37.5	1.25	0.95	1.42	0.81
		52.5	1.22	0.68	1.28	0.63
0.6	1.17	7.5	1.65	0.93	1.73	0.85
		22.5	1.47	0.71	1.50	0.67
		37.5	1.02	1.07	1.35	0.84
		52.5	0.99	1.08	1.33	0.84
0.6	1.56	7.5	1.73	1.18	1.90	1.03
		22.5	1.30	0.80	1.39	0.72
		37.5	1.32	0.85	1.43	0.76
		52.5	0.78	1.47	1.50	1.03
1.33	0.39	7.5	1.23	1.73	1.93	1.28
		22.5	1.80	1.56	2.16	1.28
		37.5	1.06	1.90	1.97	1.34
		52.5	1.15	1.30	1.58	1.00
1.33	0.78	7.5	1.57	1.35	1.88	1.11
		22.5	1.98	1.14	2.09	1.04
		37.5	1.98	1.15	2.09	1.05
		52.5	1.53	1.07	1.70	0.93
1.33	1.17	7.5	2.40	1.93	2.80	1.62
		22.5	1.72	1.65	2.17	1.32
		37.5	1.26	1.66	1.90	1.24
		52.5	1.41	0.97	1.56	0.85
1.33	1.56	7.5	2.18	1.86	2.60	1.53
		22.5	1.70	1.19	1.88	1.03
		37.5	0.91	1.85	1.86	1.29
		52.5	0.78	1.36	1.42	0.97
2.16	0.39	7.5	0.00	2.34	1.87	1.41
		22.5	1.38	2.00	2.21	1.47
		37.5	1.94	1.76	2.38	1.43
		52.5	0.61	2.02	1.85	1.33
2.16	0.78	7.5	0.00	2.31	1.84	1.39
		22.5	1.79	1.90	2.38	1.49
		37.5	1.39	1.80	2.07	1.35
		52.5	0.78	1.87	1.81	1.27
2.16	1.17	7.5	1.50	2.58	2.70	1.84
		22.5	2.33	1.49	2.52	1.33
		37.5	0.22	2.71	2.25	1.67
		52.5	0.42	2.12	1.86	1.36
2.16	1.56	7.5	0.31	3.13	2.61	1.94
		22.5	2.40	1.49	2.57	1.33
		37.5	1.36	1.84	2.09	1.37
		52.5	0.26	1.85	1.57	1.16

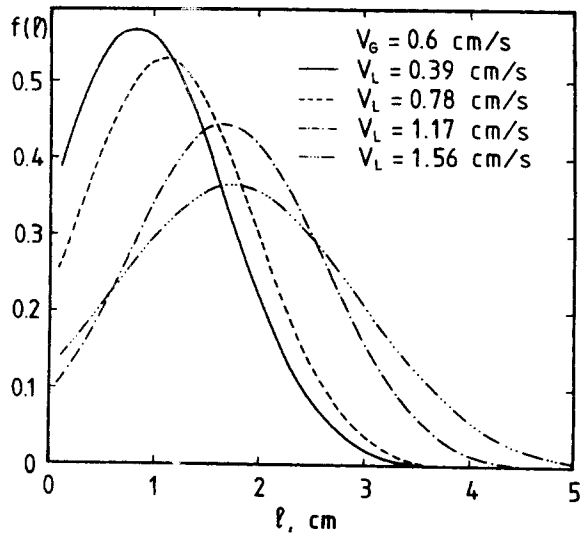

Figure 2. Effect of liquid velocity on differential bubble length distribution in three-phase fluidized bed.

$V_G = 0.6$ cm/s, $r/R = 0$, $z = 7.5$ cm

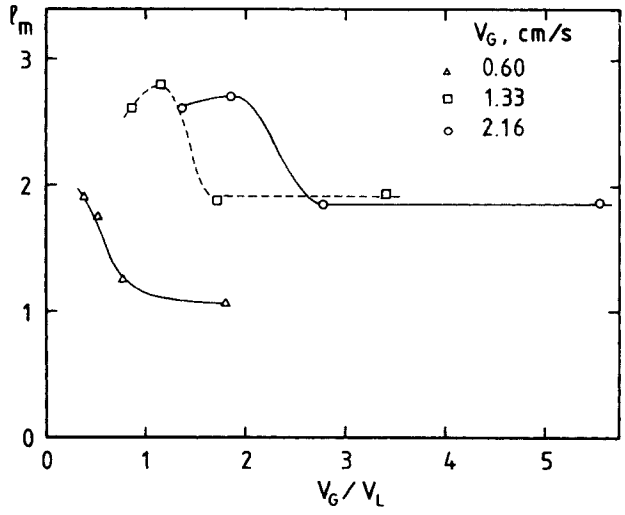

Figure 3. Effect of V_G/V_L ratio on initial mean bubble length.

$z = 7.5$ cm

can be distinguished. At low liquid velocities, $V_L = 0.39$ and 0.78 cm/s, the grid level bubble length distributions are quite skewed and their variances are quite similar. Furthermore, the grid level bubble length distributions become more symmetrical at high liquid velocities ($V_L = 1.17$ and 1.56 cm/s) and their variances increase. This phenomenon is more pronounced at higher gas velocities.

The asymmetry of the grid level bubble length distributions increased progressively as the liquid velocity decreased, and this behavior may be explained by bubble formation at the gas injector. At low gas and liquid velocities, gas bubbles formed freely in a close-to-stagnant flow field and detached from the injector in a series fashion, one after another, without strong interaction between bubbles. Therefore, narrow grid level bubble length distributions with small mean bubble lengths could be observed. With the combination of low gas velocity (0.6 cm/s) and high liquid velocities (1.17 and 1.56 cm/s), a wider grid level bubble length distribution with a larger mean bubble length was observed. The later bubbles could be entrained by the liquid jet to coalesce with the former bubbles in a train of bubbles before these former bubbles had the chance to accelerate, and rose freely in the fluidized bed. When the gas velocity increased at low liquid velocity, jetting phenomenon occurred at the gas injector. Grid level bubble length distributions became wider and the mean bubble length became larger. At high gas and liquid velocities there was even higher opportunity for larger bubbles to be formed due to the combined effect of liquid jet on more gas bubbles. Therefore, bubble length distributions became even wider, and larger mean bubble lengths were observed.

The grid level bubble lengths in the fluidized bed are influenced by the operating condition, defined as the V_G/V_L ratio. Mean bubble lengths, ℓ_m, at the grid level for various conditions are shown in Figure 3. It was observed that larger grid level bubbles were promoted by high liquid flow rate, that is, low V_G/V_L ratio. For example, as illustrated in Figure 3, the mean bubble length increased gradually as V_G/V_L decreased. Conversely, the mean bubble length decreased toward an asymptotic value as the liquid velocity decreased or the equivalent V_G/V_L became bigger. Moreover, for $V_G = 1.33$ and 2.16 cm/s, the mean bubble length decreased toward similar asymptotic values, around 1.95 cm, as V_G/V_L increased. In summary, the increase of the V_G/V_L ratio at a constant V_G value reduces the initial sizes, providing smaller and stable bubbles. The difference in stable bubble sizes for high (1.33 and 2.16 cm/s) and low (0.6 cm/s) gas velocities may be explained by bubble formation at the injector, as described earlier.

Another interesting observation from Figure 3 concerns the different ℓ_m values at constant V_G/V_L obtained with a simultaneous change of V_L and V_G. For example, at $V_G/V_L = 2$ a combination of higher V_L and V_G values, $V_L = 1.17$ and $V_G = 2.16$, favors larger bubbles. This fact can be visualized when the ℓ_m value for these conditions, about 2.7 cm, is compared with the ℓ_m values, about 2 cm and 1 cm, obtained for $V_L = 0.78$ cm/s and $V_G = 1.33$ cm/s, and for $V_L = 0.39$ cm/s and $V_G = 0.6$ cm/s, respectively.

Upper levels

The truncated normal bubble length distributions were observed throughout the fluidized bed as gas bubbles rose. The evolution of bubble length distributions in the fluidized bed is influenced by the operating conditions, such as the gas and the liquid velocities. An example of the steady-state evolution of the bubble length distribution at the centerline of the fluidized bed is shown in Figure 4 for $V_G = 0.6$ cm/s, and $V_L = 0.39$ cm/s. A progressive increase in mean bubble length as bubbles rose in the fluidized bed was observed at low liquid velocity ($V_L = 0.39$ cm/s), as shown in Figure 4. This evolution was understood as an indicator of the existence of the coalesced bubble regime. However, mean bubble lengths decreased slightly and the bubble length distributions became narrower at the highest measuring level, located at 52.5 cm above the distributor, just below the upper surface of the fluidized bed. This phenomenon may be related to the solid holdup profiles in the fluidized beds. It has been shown in previous studies that the solid holdup

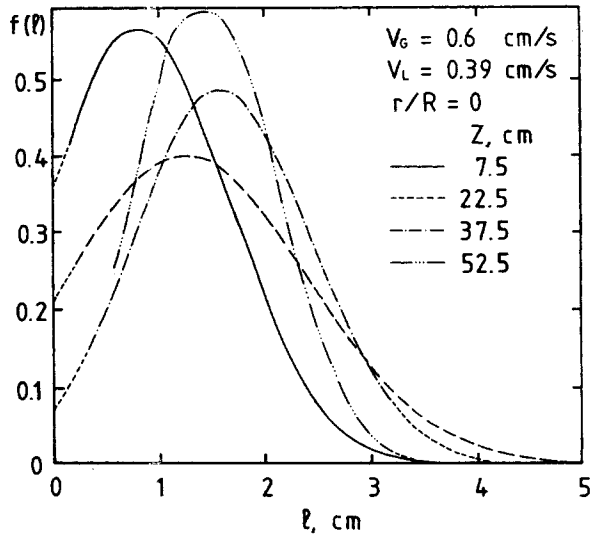

Figure 4. Bubble length distributions in three-phase fluidized beds.
$V_G = 0.6$ cm/s, $V_L = 0.39$ cm/s, $r/R = 0$

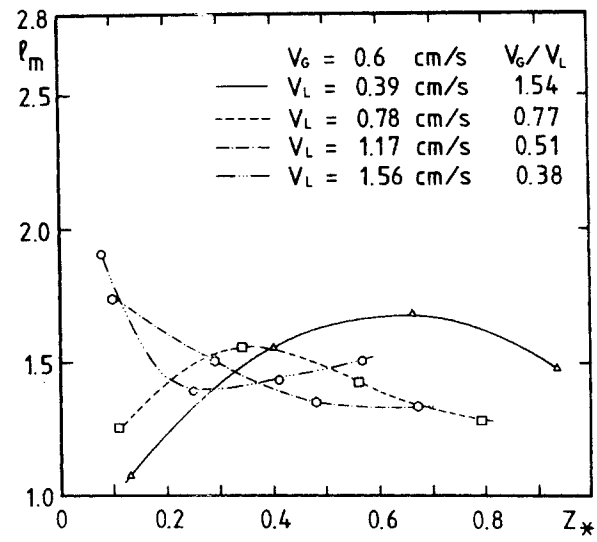

Figure 5. Effect of liquid velocity on mean bubble length.
$V_G = 0.6$, $r/R = 0$

decreases dramatically in the top part of a three-phase fluidized bed (Lee and de Lasa, 1987). Therefore, bubble breakage can be expected as a result of lower apparent bed viscosity. Similar patterns of bubble coalescence and redispersion at $V_L = 0.39$ cm/s were observed, as documented in Table 1, for higher gas velocities ($V_G = 1.33$ and 2.16 cm/s). Therefore it can be concluded that bubble coalescence occurs in the bed if the initial bubble size is small enough.

On the other hand, bubble breakup happens if large bubbles are injected. The bubble breakup evolution pattern was understood as an indicator of the existence of the dispersed bubble regime. For $V_L = 1.56$ cm/s the mean bubble length decreased with height, as shown in Table 1, for $V_L = 1.56$ cm/s and $V_G = 1.33$ cm/s. In fact, the mean bubble length was reduced from 2.60 to 1.42 cm. It was observed that there was a tendency for bubbles to rearrange themselves toward a final size, possibly related with a mechanical equilibrium configuration. These observations show how the gas injection system plays an important role on the bubble flow pattern evolution in a three-phase fluidized bed.

Mean bubble lengths along the centerline of the fluidized bed are shown in Figure 5 for $V_G = 0.6$ cm/s and $V_L = 0.39$ to 1.56 cm/s. As illustrated in Figure 5, the bubble flow evolutions were clearly dominated by the liquid velocity. Additional information concerning the change of the mean bubble length with position for other conditions studied is given in Table 1. Bubble coalescence (increase of ℓ_m) occurred at low liquid velocities while bubble dispersion (decrease of ℓ_m) took place at high liquid velocities. Bubble redispersion at low liquid velocities occurred only in the top section of the fluidized bed. The differences in mean bubble length along the fluidized bed were relatively small at low gas velocities. However, as documented in Table 1, the changes of bubble length with axial position became significantly larger at higher gas velocities.

Radial profiles of mean bubble length were measured at low liquid velocity ($V_L = 0.39$ cm/s). It was found that these profiles were rather flat in the center region of the column where most of the gas bubbles were detected. These results are consistent with measurements performed at the centerline of the column. Bubble length distributions became wider and mean bubble lengths became larger at higher axial locations and at various radial positions. Moreover, redispersion occurred as expected and smaller mean bubble length was observed when bubbles approached the top measuring level of the fluidized bed ($z = 52.5$ cm). Furthermore, measurements of mean bubble length, across the bed radius, at higher liquid velocity ($V_L = 1.56$ cm/s) also confirmed a consistent tendency of decreasing ℓ_m profiles with increasing axial height results. This is in agreement with the bubble breakup process. (Additional results concerning radial profiles are given as supplementary material.)

The bubble flow evolutions in the present study are qualitatively coincident with the type of flow regime diagrams developed by Muroyama et al. (1978) and Muroyoma and Fan (1985). However, a detailed comparison with previous reports is not possible for the particle size and type of solid (glass beads) used in this study. The flow regime maps reported previously were developed for glass beads bigger than, or equal to 1 mm. In Figure 6, available data from previous studies are collected. The solid circles in Figure 6 represent the operating conditions of this study at $V_G = 0.6$ cm/s. The upper two experimental points ($V_L = 1.17$ and 1.56 cm/s) were found to be in the dispersed bubble regime while the lower two points ($V_L = 0.78$ and 0.39 cm/s) corresponded to the coalesced bubble regime. Therefore, the transition for particles of 250 μm, shown as a dashed zone in Figure 6, should be between $V_L = 0.78$ and 1.17 cm/s. An interesting fact can be pointed out in referring to this figure: as the particles increase in size, beyond the so-called critical particle size (close to 3 mm), their transition between coalesced and dispersed bubble flow patterns approaches the minimum fluidization velocity. Since the flow patterns have been characterized by visual observation, the possibility of the existence of a coalesced bubble regime at liquid velocities close to minimum fluidization might not be noticed. It can also be observed in Figure 6 that below the critical size, a function suitable for the transition between bubble coalescence and dispersion regimes

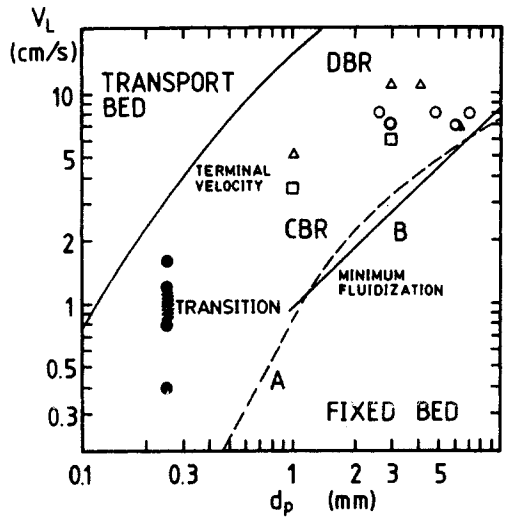

Figure 6. Transition between coalesced bubble regime (CBR) and dispersed bubble regime (DBR), air–water–glass bead system.

Data from: ○ Muroyama et al. (1978), △ Fan et al. (1985), □ Fan et al. (1987), ● present study

— — — A: correlation by Wen and Yu (1966), ——— B: correlation by Riba et al. (1978) for minimum fluidization

Upper continuous line: terminal velocity for a single particle in the liquid

should have a somewhat similar shape than the minimum fluidization and the terminal velocity of the single particle.

Acknowledgment

The financial support of the National Science and Engineering Research Council of Canada is highly appreciated. A. Soria was awarded a Ph.D. Scholarship from the Consejo Nacional de Ciencia y Tecnología, México.

Notation

$E(\ell)$ = mean of truncated normal distribution
$f(\ell)$ = truncated normal bubble length distribution
ℓ = bubble length, cm
ℓ_m = mean bubble length, cm
r = radius, cm
R = radius of the fluidized bed, cm
$t = (\ell - \mu)/\sigma$
Var (ℓ) = variance of the truncated normal bubble length distribution
V_G = superficial gas velocity defined at room temperature and bed pressure, cm/s
V_L = superficial liquid velocity, cm/s
z = axial height, cm

Greek Letters

μ = location parameter of the truncated normal distribution, cm
σ^2 = scale parameter of the truncated normal distribution, cm^2
Φ = cumulative standard normal distribution

Literature Cited

Fan, L. S., A. Matsura, and S. H. Chern, "Hydrodynamic Characteristics of a Gas–Liquid–Solid Fluidized Bed Containing a Binary Mixture of Particles," *AIChE J.*, **31**, 180 (1985)

Fan, L. S., K. Kitano, and B. E. Kreischer, "Hydrodynamics of Gas–Liquid–Solid Annular Fluidized Bed," *AIChE J.*, **33**(2), 225 (1987)

Lee, S. L. P., and H. I. de Lasa, "Phase Holdups in Three-Phase Fluidized Beds," *AIChE J.*, **33**(8), 1359 (1987).

———, "Application of a Dispersion Model for Bubble Dynamics in Three-Phase Fluidized Beds," *Fluidization*, **VI**, 531 (1989).

Lee, J. C., A. J. Sherrard, and P. S. Buckley, "Optimum Particle Size in Three-Phase Fluidized Bed Reactors," *Fluidization and Its Applications*, H. Angelino, ed., Cepadues Editions, Tolouse, 407 (1974).

Lee, S. L. P., H. de Lasa, and M. A. Bergougnou, "Bubble Measurement in Three-Phase Fluidized Beds Using a U-Shaped Optical Fiber," *Can. J. Chem. Eng.*, **62** (2), 165 (1984).

Muroyama, K., and L. S. Fan, "The Fundamentals of Gas–Liquid–Solid Fluidization," *AIChE J.*, **31**(1), 1 (1985).

Muroyama, K., K. Hashimoto, T. Kawabata, and M. Shiota, "Axial Liquid Mixing in Three-Phase Fluidized Beds," *Kagaku Kogaku Ronbunshu*, **4**(6), 622 (1978).

Riba, J. P., Routie, and J. P. Couderc, "Conditions Minimales de Mise en Fluidisation par un Liquide," *Can. J Chem. Eng.*, **56**, 26 (1978).

Wen, C. Y., and Y. H. Yu, "Mechanics of Fluidization," *Chem. Eng. Prog. Symp. Ser.*, **62**(62), 100 (1966).

See NAPS document no. 04808 for 16 pages of supplementary material. Order from NAPS c/o Microfiche Publications, P.O. Box 3513, Grand Central Station, New York, NY 10163. Remit in advance in U.S. Funds only $7.75 for photocopies or $4.00 for microfiche. Outside the U.S. and Canada, add postage of $4.50 for the first 20 pages and $1.00 for each of 10 pages of material thereafter, $1.50 for microfiche postage.

Manuscript received Jan. 16, 1990, and revision received Aug. 31, 1990.